HOSTED BY
ELSEVIER
CrossMark
Available online at www.sciencedirect.com
ScienceDirect
Defence Technology 12 (2016) 227–233
www.elsevier.com/locate/dt

# Investigation on the flow control of micro-vanes on a supersonic spinning projectile

Jie MA *, Zhi-hua CHEN, Zhen-gui HUANG, Jian-guo GAO, Qiang ZHAO

*Key Laboratory of Transient Physics, Nanjing University of Science and Technology, Nanjing 210094, China*

Received 5 July 2015; revised 8 January 2016; accepted 21 January 2016

Available online 26 February 2016

**Abstract**

Studies have shown that micro-wedge vortex generators (MVG) can effectively control the flow separation of supersonic boundary layer. In order to improve the flight stability of spinning projectile, the original standard 155 mm projectile was taken as an example, and the micro-vanes were mounted at the projectile shoulder to investigate the separation control on the aerodynamic characteristics of projectile. Numerical simulations were performed with the use of DES method for the flow fields of projectiles with and without micro-vanes, and the characteristics of the boundary layer structures and aerodynamic data were compared and discussed. Numerical results show that the micro-vanes can be used to inhibit separation of fluid on projectile surface, and improve the flight stability and firing dispersion of projectile.


*Keywords:* Spinning projectile; Micro-vane; Stability; Aerodynamic characteristics; Fluid control

## 1. Introduction

Precision strike is a general trend in modern warfare, and many countries in the world improve the flight stability and firing dispersion of projectile mainly through the development of guided munitions and transformation of conventional ammunition [1]. Supersonic spinning projectiles are greatly influenced by boundary layer separation in the process of flight [1,2]. The flight stability of a projectile is one of the basic requirements of the projectile design [3], which it means that its angle of attack between the axis of the projectile and velocity vector should be within a certain limit, and gradually decay [4–6].

Micro-vanes are found to be able to suppress the separation of supersonic flow. In this paper, in order to further improve the flight stability of the standard 155 mm projectile [7], the micro-vanes were mounted at the projectile shoulder according to the Task Force findings [8–10], so that the fluid separation in the boundary layer of projectile can be suppressed, and the projectile has a stronger anti-interference ability during flight for improving its flight stability and firing accuracy. The supersonic flow structure around micro-vanes and the control mechanism of boundary layer separation were discussed in detail in Refs. [8–10].

Numerical simulations were performed with the use of DES method for the flow fields of 155 mm standard projectiles for two cases with and without micro-vanes. The modifications of the boundary layer structures and aerodynamic data for two cases were compared and discussed. Numerical results show that the micro-vanes can be used to inhibit the fluid separation of projectile surface, improve the projectile lift and pitching moment, and eliminate the shaking of lift and pitching moment, as a result of improving the flight stability and firing dispersion, which can provide guidance for the improvement of supersonic projectiles.

## 2. Investigation approach

The fluid field of supersonic spinning projectile was simulated based on DES simulation method. Realizable $k-\varepsilon$ turbulence model is used for the near wall region, and the large eddy simulation (LES) is used for external flow field, in which the spatial discrete are discretized using the finite volume method, the convection term is approached with the second order AUSM format, and a central difference scheme is used for the viscosity term.

The transport equations of turbulent kinetic energy and dissipation in realizable $k-\varepsilon$ turbulence model are

Peer review under responsibility of China Ordnance Society.
* Corresponding author.
*E-mail address:* majie19910@163.com (J. MA).

http://dx.doi.org/10.1016/j.dt.2016.01.008

$$\frac{\partial(\rho k)}{\partial t}+\frac{\partial(\rho k u_i)}{\partial x_i}=\frac{\partial}{\partial x_j}\left[\left(\mu+\frac{\mu_t}{\sigma_k}\right)\frac{\partial k}{\partial x_j}\right]+G_K+G_b-\rho\varepsilon-Y_M \tag{1}$$

$$\frac{\partial(\rho\varepsilon)}{\partial t}+\frac{\partial(\rho\varepsilon u_i)}{\partial x_i}=\frac{\partial}{\partial x_j}\left[\left(\mu+\frac{\mu_t}{\sigma_\varepsilon}\right)\frac{\partial\varepsilon}{\partial x_j}\right]+\rho C_1 E\varepsilon - \rho C_2\frac{\varepsilon^2}{k+\sqrt{\nu\varepsilon}}+C_{1\varepsilon}\frac{\varepsilon}{k}C_{3\varepsilon}G_b \tag{2}$$

The control equations of LES model can be obtained by filtering Navier–Stokes equations in wave number space or irrational space. The filtration process is to remove the small vortexes which are shorter than filter width or a given unreasonable width. The resulting control equations of maelstrom are

$$\frac{\partial\rho}{\partial t}+u\frac{\partial\rho\overline{u_i}}{\partial x_i}=0 \tag{3}$$

$$\frac{\partial}{\partial t}(\rho\overline{u_i})+\frac{\partial}{\partial x_j}\left(\rho\overline{u_i u_j}\right)=\frac{\partial}{\partial x_j}\left(u\frac{\partial\overline{u_i}}{\partial x_j}\right)-\frac{\partial\overline{p}}{\partial x_j}-\frac{\partial\tau_{ij}}{\partial x_j} \tag{4}$$

where $\tau_{ij}$ is defined as subgrid stress, $\tau_{ij}=\rho\overline{u_i u_j}-\rho\overline{u}_i\overline{u}_j$.

A sliding mesh needs to be used in order to simulate the flight state of spinning projectile. Sliding grid technology requires an external fixed area and inner motion area round the projectile, with a pair of interfaces being between two areas, and the points of the interface grid do not need to overlap; they only need to do numerical interpolation on the slip boundary to ensure the flux conservation between two regions, and the deformation of grid cell in motion, do not occur. Therefore the sliding grid technology occupies less memory of computer, calculates fast and has high precision.

155 mm M549 projectile, as shown in Fig. 1(a), was used as an example in the present paper. The micro-vanes were mounted at the projectile shoulder to form a new physical model, as shown in Fig. 1(b). Fig. 2 shows the computational

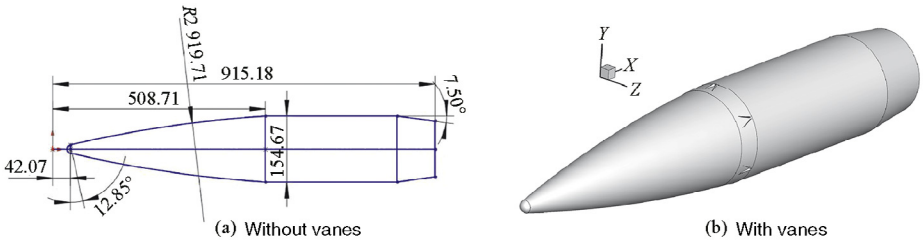


Fig. 1. M549 projectile [7].

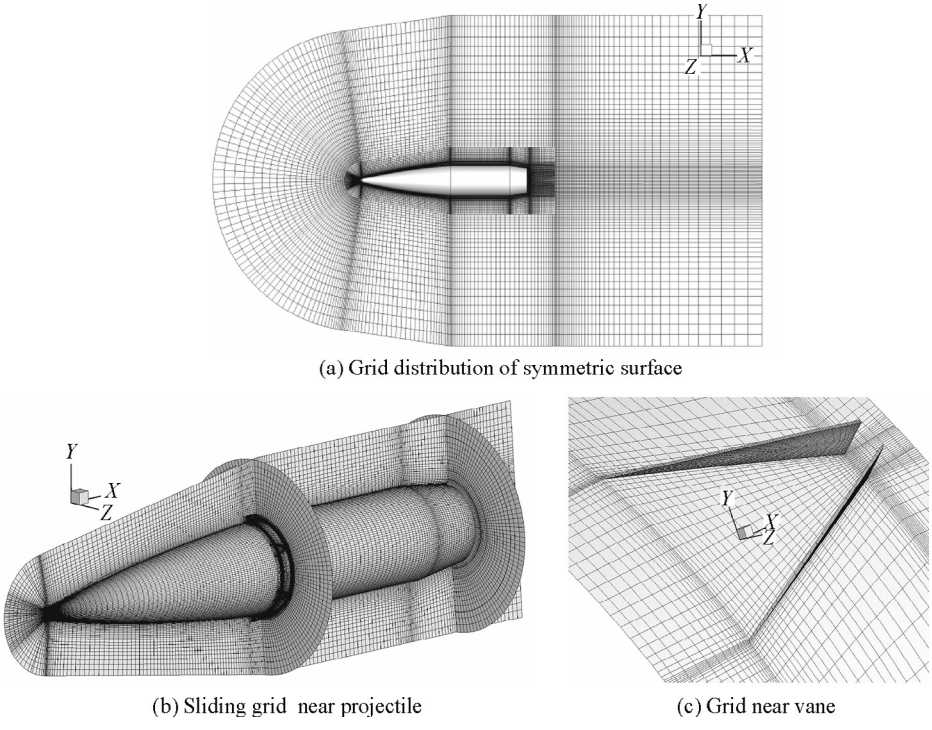


Fig. 2. Grid around the projectile.

domain of M549 projectile. Fig. 2(a) shows the grid distribution of symmetric surface, and Fig. 2(b) and (c) show the sliding grid near the projectile and the grid near a vane, respectively. The computational domain is divided into an external fixed area and an internal sliding area. The grids within boundary layer were refined along the normal direction, and the grids near the head, shoulder and tail of projectile were refined along the flow direction. After repeated calculations and convergence tests, the grid number of the whole area is about 2 million.

Projectile surface is applied with the no-slip wall boundary condition, and the meshes of the interior layers are designed to move with the projectile. The interfaces of external fixed grid area and internal sliding area are adopted with the sliding boundary conditions. The mach number of incoming flow is assumed to be 2.05. The initial pressure $P_0$ is set to $1.014 \times 10^5$ Pa, and the initial temperature $T_0$ is 278K. The spin rate of the projectile is chosen to be $\Omega = 1112$ rad/s, which equals a maximal dimensionless spin rate, $pD / 2U_\infty = 0.154$. The rotation is anti-clockwise viewing from the base of the projectile.

## 3. Results and discussion

Fig. 3 shows the comparison of previous measured and simulated side force coefficients of a generic 6.37 diameter long tangential-ogive-cylinder type projectile. The simulated results of unsteady DES method are compatible with the previous simulated and experimental results. It verifies that the credibility of the numerical simulation results in this paper.

Fig. 4 shows the pressure distributions on the surfaces of the standard projectile and the projectile with micro vanes and around them with *Ma* of 2.05 and angle of attack (AOA) of 4°. The main shock wave structures are the same for both cases; there are oblique shock waves around the heads and expansion waves near the tails. But for the projectile with micro-vanes, the oblique shock wave also forms along the micro-vanes, and its strength is much weaker than that of head shock wave. In addition, the shock waves around micro-vanes are stronger at the area close to the windward side, which makes the surface pressure higher than that on the leeward side, and leads to a raise in the projectile lift.

### 3.1. Control mechanism of micro-vanes

Micro-vortex generator is considered to be one of the most applicable prospects in the field of supersonic and hypersonic flow control. It can generate a strong vortex pair under the action of windward airflow. The vortex structures can inhale the high-speed gas of mainstream into the boundary layer, and push the original low speed gas of the boundary layer flow into the main flow, thus increasing the momentum boundary layer and turning an adverse pressure gradient of flow separation into a favorable pressure gradient. The flow separation of boundary layer can be suppressed [10].

A series of studies about tail vortexes of micro-vane had been carried [10]. The basic structure of micro-vane is shown in Fig. 5, and the structure parameters of micro-vane are $h = 2$ mm, $a = 7.5$ mm, $b = 1.25$ mm, $c = 13.05$ mm.

It can be seen from Fig. 6 that the wake flow structures are simple; there is mainly a counter-rotating streamwise vortex-pair which suggests the main mechanism of the boundary layer control. The streamwise vortex tube can also entrain high

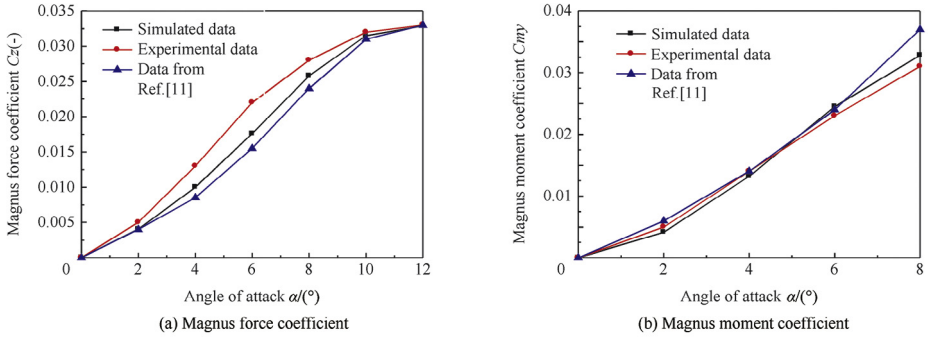


Fig. 3. Comparison of the measured Magnus coefficient and the simulated results of a tangential-ogive-cylinder type projectile for $Ma = 3$ [11,12].

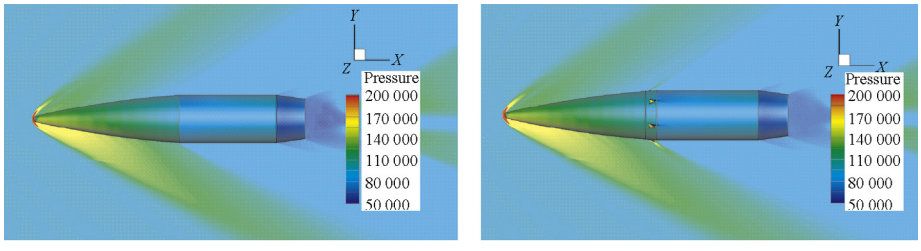


Fig. 4. Pressure distributions of (a) the standard projectile and (b) the projectile with micro-vanes for $Ma = 2.05$, $\Omega = 1112$ rad/s and $AOA = 4°$.

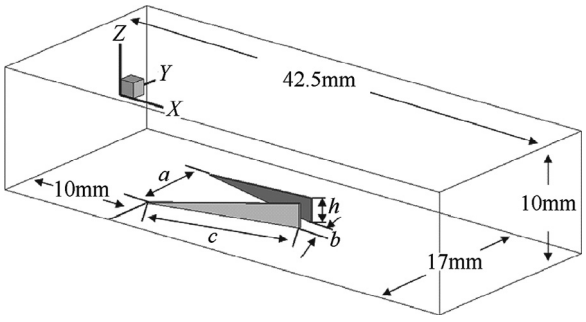


Fig. 5. Computational model of micro-vane.

momentum gas from the free stream into the boundary layer and redistribute the pressure distribution on the boundary layer.

Fig. 7 shows the vorticity distribution on the cross sections of the projectiles without and with micro-wedge for $Ma = 3$, $AOA = 4°$ and spin rate $\Omega = 157$ rad/s. It can be seen from Fig. 7 that the vorticity distribution behind vanes on the projectile with micro-vanes is different from that on the standard projectile. As shown in Fig. 7(c), the counter-rotating streamwise vortex-pair attaches on the surface of projectile. Its effect is consistent with the details described in Ref. [4]. The vortex structure can inhale the high-speed gas of mainstream into the boundary layer, and push the original low speed gas of the boundary layer into the outer main flow. So far, the energy exchange between them is completed, and the fluid separation on the surface of projectile is inhibited.

Fig. 8 shows the density isosurfaces of projectiles without and with vanes for $Ma = 2.05$ and $AOA = 0°$, and the colors of the isosurface represents pressure value. It can be seen from Fig. 8 that the typical streamwise vortex pair behind the micro-vanes is distributed along the body of projectile, and the trailing vortexes distribute spirally due to the rotation of projectile. The leeward pressure of projectile is slightly decreased after adding the micro-vanes; therefore the projectile lift is enhanced. It can also be seen from Fig. 8 that the counter-rotating streamwise vortex pairs form the buffering zones. It is conducive to weaken

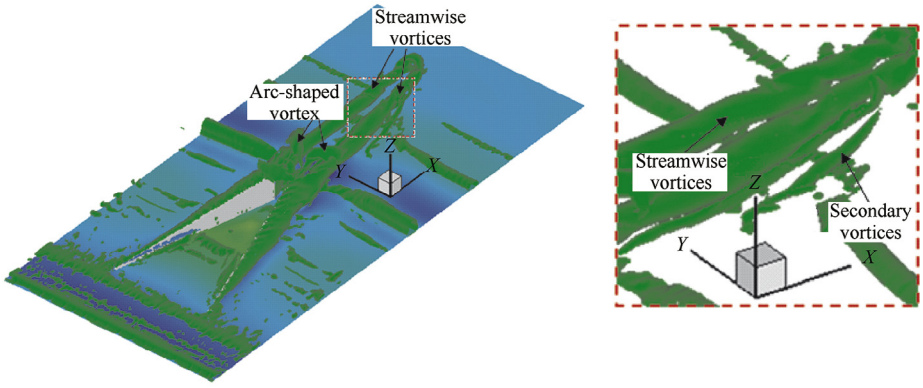


Fig. 6. Vortex rings shown by iso-surface of $\lambda_2$ [10].

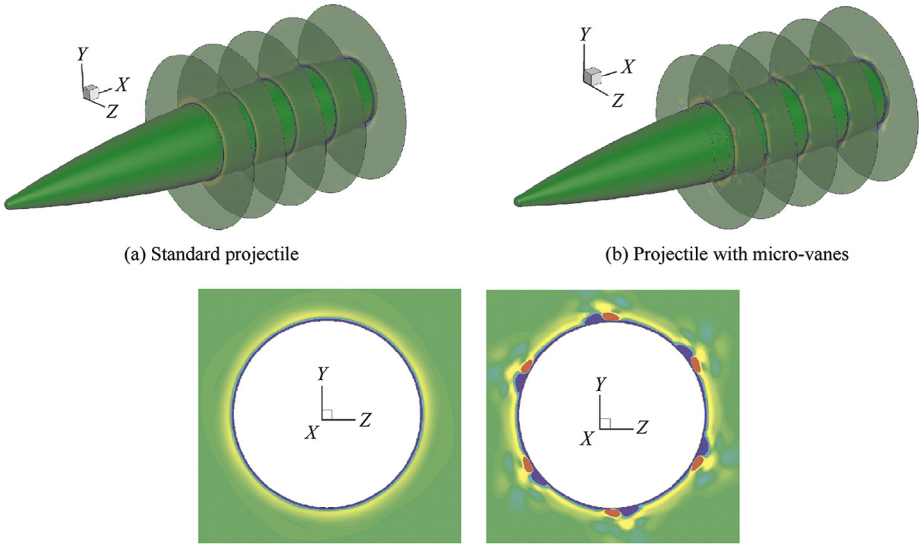


(a) Standard projectile

(b) Projectile with micro-vanes

(c) Vorticity distribution at the point of $x/D$=2.87

Fig. 7. The vorticity distributions on cross sections of the projectiles without and with micro-wedge for $Ma = 2.05$, $AOA = 0°$ and spin rate, $\Omega = 1112$ rad/s.

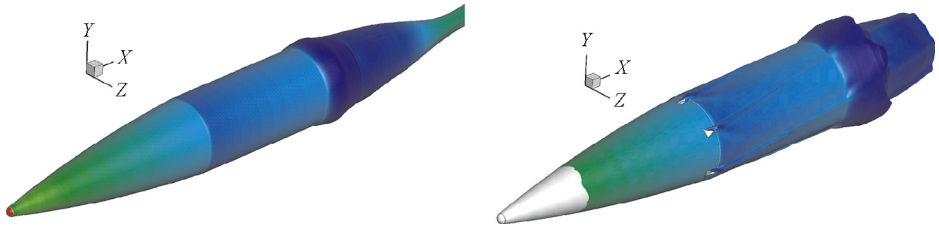


Fig. 8. Density isosurfaces ( $\rho = 0.95\ \mathrm{kg/m^3}$) of projectiles without and with vanes for $Ma = 2.05$ and $AOA = 0°$.

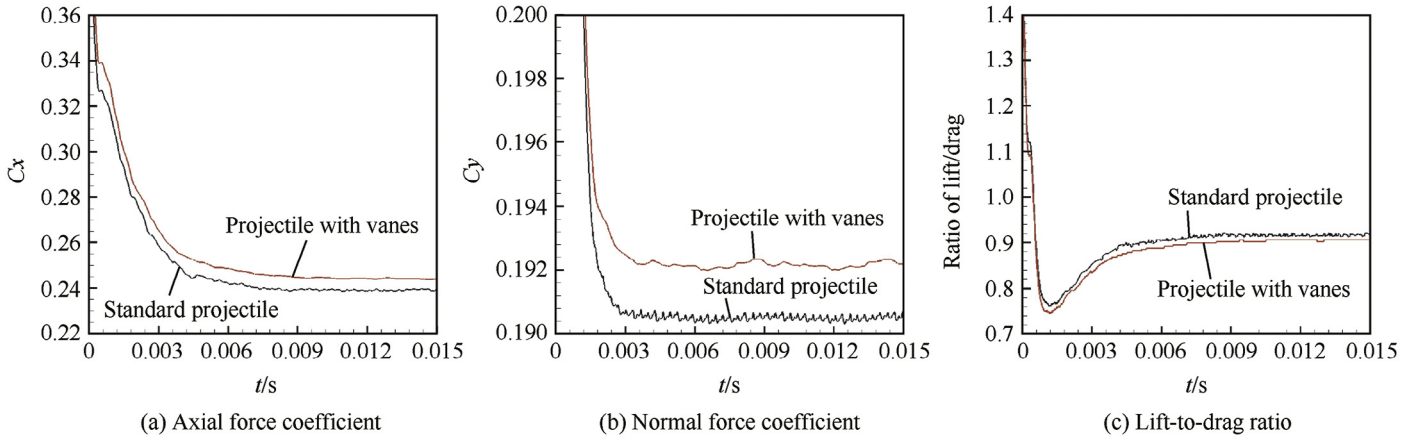


Fig. 9. Comparison of aerodynamic coefficients of projectile with and without vanes for $Ma = 2.05$ and $AOA = 4°$.

the interference encountered during flight so as to improve its flight stability.

### 3.2. The influence of micro-vanes on aerodynamic coefficient

Figs. 9 and 10 show the comparison of aerodynamic coefficients of the projectiles with and without vanes for $Ma = 2.05$ and $AOA = 4°$. The aerodynamic coefficients of projectile with micro-vanes increase slightly. However, the obvious slight cyclical fluctuations can be observed from the curve of aerodynamic coefficient versus time, but the aerodynamic coefficient becomes stable after the addition of micro-vanes. And the normal coefficient of projectile with vanes increases and eliminates its oscillation so as to improve the stability, but decrease the lift-to-drag ratio. Generally, vibration of aerodynamic coefficients is mainly caused by fluid separation on the projectile surface. Separation vortex shedding from the projectile surface will cause pressure pulsation on the projectile surface, leading to the vibration of the aerodynamic force coefficient. However, aerodynamic coefficient changed smoothly after adding the micro-vanes, and it also can illustrate that fluid separation on the projectile surface has been suppressed.

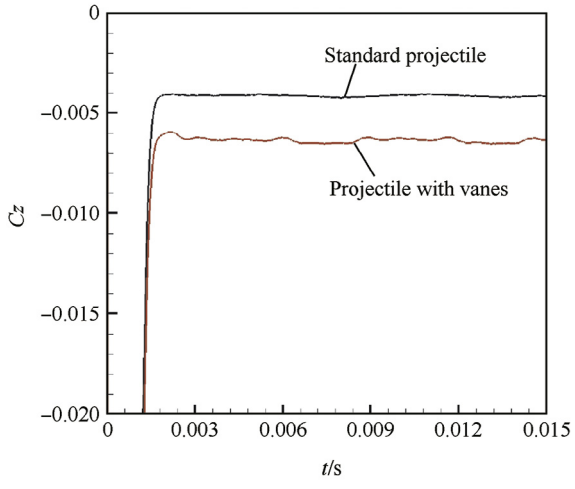


Fig. 10. Comparison of Magnus coefficients of projectiles with and without vanes at $Ma = 2.05$ and $AOA = 4°$.

Fig. 11 shows the comparison of aerodynamic moment coefficients of projectiles with and without vanes for $Ma = 2.05$ and $AOA = 4°$. It can be found from Fig. 11 that Magnus moment coefficient changes little after adding the micro-vanes. Meanwhile, the rolling moment coefficient of the projectile with micro-vanes increases, but the increase in rolling moment coefficient is very small and close to zero. Pitching moment of the projectile with micro-vanes increases and becomes stable, which means the projectile can return to the equilibrium state more quickly. Therefore, the addition of micro-vanes can improve the flight stability and fire dispersion of spinning projectiles.

In order to give a much broader scope of Mach numbers for a complete analysis, the normal force coefficient and pitching moment coefficient which are the typical parameters for $AOA = 4°$ and $Ma = 1.2$ and $Ma = 4$ in the present paper are shown in Figs. 12 and 13. However, the obvious cyclical fluctuations cab be observed from the curves of aerodynamic

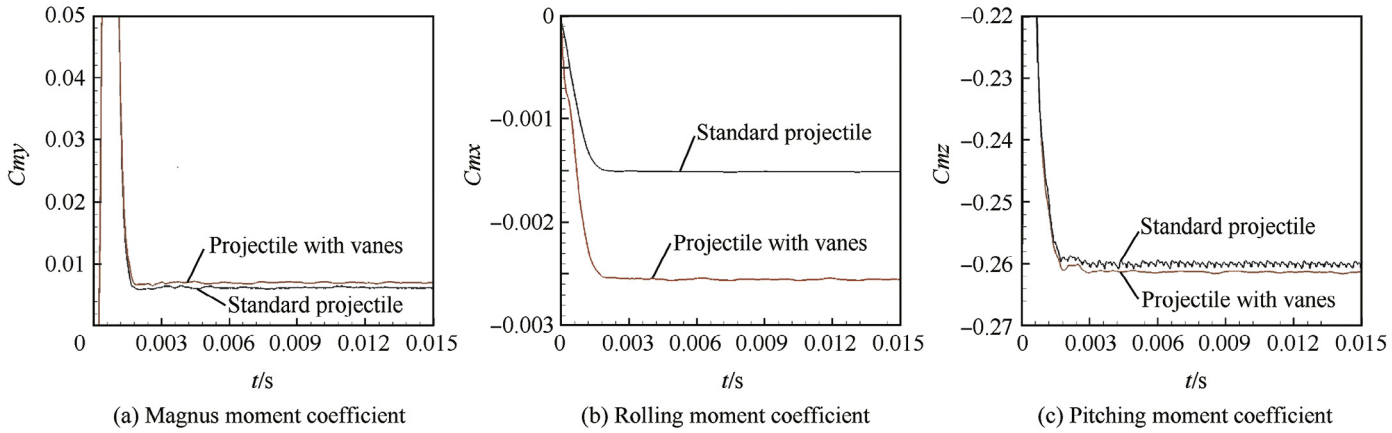


Fig. 11. Comparison of aerodynamic moment coefficients of projectiles with and without vanes for $Ma = 2.05$ and $AOA = 4°$.

coefficient versus time in Figs. 12 and 13, but the aerodynamic coefficient becomes stable after the addition of micro-vanes. As can be seen from Fig. 13, there is a smaller vibration about the aerodynamic coefficients of projectile for $Ma = 4$. It can be found by comparing Figs. 12, 13 and 9 that the vibration amplitude of aerodynamic force coefficient decreases and the vibration frequency increases gradually with the increase in Mach number. However, the control of micro-vanes can inhibit the fluid separation on the surface of projectile and improve its flight stability and firing dispersion.

The vibration of aerodynamic force and moment coefficients is mainly caused by the fluid separation on the surface of projectile. The separation vortexes shed from the surface of projectile may cause the fluctuation of pressure on the surface of projectile and the vibration of aerodynamic coefficients. However, the aerodynamic coefficients become smooth after mounting the micro-vanes on a projectile, and it illustrates that the fluid separation on the surface of projectile is suppressed, which is beneficial for improving the flight stability of spinning projectile.

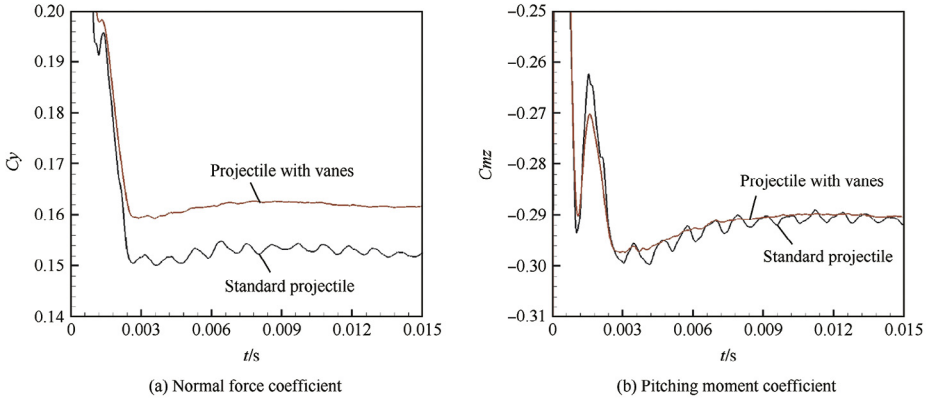


Fig. 12. Comparison of aerodynamic coefficients of projectiles with and without vanes for $Ma = 1.2$ and $AOA = 4°$.

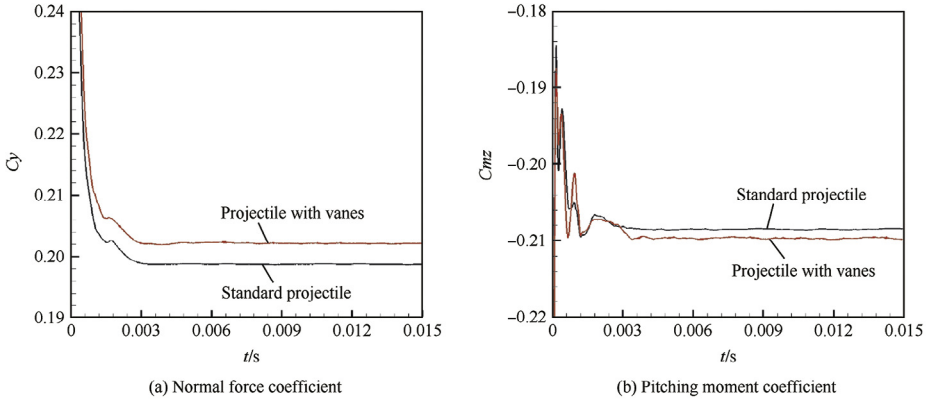


Fig. 13. Comparison of aerodynamic coefficients of projectiles with and without vanes for $Ma = 4$ and $AOA = 4°$.

## 4. Conclusion

Numerical simulations were performed with the use of DES method for the flow fields of 155 mm standard projectiles with and without micro vanes, and the modifications of the boundary layer structures and the aerodynamic data for two cases were compared and discussed. The numerical results show that a counter-rotating streamwise vortex pair behind each vane attaches on the surface of projectile and it can inhibit the flow separation along the body of projectile. In addition, Magnus force and roll moment increase slightly after adding the micro vanes, and have smaller impact on the flight stability of projectile than lift and pitching moment so that they can be neglected basically. Meanwhile, the normal force coefficient and pitching moment coefficient of the projectile become stable, obviously and virtually eliminating the fluctuation term over time so that the projectile gains the ability of anti-interference, and the flight stability and fire dispersion can be improved.

## References

[1] Rausch JR, Roberts BB. Reaction control system plume flow field interaction effects on the space shuttle orbiter. San Diego: Proceedings of 10th AIAA and SAE Propulsion Conference; 1974.

[2] Srivastava B. Aerodynamic performance of supersonic missile body and wing tip mounted lateral jets. J Spacecr Rockets 1998;35(3):278–86.

[3] Wu X, Wang J, Wu X, Geng G. The numerical computational for external flow field of artillery projectile with side jet flow. J Propuls Technol 1998;19(3):57–60.

[4] Margason RJ Fifty years of jet in CROSS flow research in AGARD Symposium: on a Jet in Cross Flow; AGARD CP- 534.

[5] Selby GV, Lin JC, Howard EG. Control of low-speed turbulent separated flow using jet vortex generators. Exp Fluids 1992;12:394–400.

[6] Han Z. External ballistic of projectiles and missiles, vol. 7. Beijing Institute of Technology Press; 2008. p. 150–3.

[7] Nietubicr CJ, LaFarge RA. Aerodynamic coefficient predictions for a projectile configuration at transonic speeds. 22nd Aerospace Sciences Meeting, Aerospace Sciences Meetings 1984;AIAA-84-0326.

[8] Xue D, Chen Z, Sun X. Investigations on the flow characteristics of supersonic flow past a micro-ramp. Eng Mech 2013;30(4):455–9, [in Chinese].

[9] Xue D, Chen Z, Sun X. Micro-ramp control of the boundary separation induced by the flow past an airfoil. Eng Mech 2014;31(8):217–22, [in Chinese].

[10] Xue D, Chen Z, Jiang X. Numerical investigations on the wake structures of micro ramp and vanes. Fluid Dyn Res 2014;46:015505.

[11] Kalatt D, Hruschka R, Leopold F. Numerical and experimental investigation of the magnus effect in supersonic flows. New Orleans, Louisiana: Aerodynamics Conference; 2012. p. AIAA-2012-3230.

[12] Ma J, Chen Z. Effects of the boattail of a spinning projectile on its aerodynamics characteristics. 5TH ICMEM, 2014; 89–94.